RESEARCH ARTICLES

The Emperor Seamounts: Southward Motion of the Hawaiian Hotspot Plume in Earth's Mantle

John A. Tarduno,[1]* Robert A. Duncan,[2] David W. Scholl,[3] Rory D. Cottrell,[1] Bernhard Steinberger,[4] Thorvaldur Thordarson,[5] Bryan C. Kerr,[3] Clive R. Neal,[6] Fred A. Frey,[7] Masayuki Torii,[8] Claire Carvallo[9]

The Hawaiian-Emperor hotspot track has a prominent bend, which has served as the basis for the theory that the Hawaiian hotspot, fixed in the deep mantle, traced a change in plate motion. However, paleomagnetic and radiometric age data from samples recovered by ocean drilling define an age-progressive paleolatitude history, indicating that the Emperor Seamount trend was principally formed by the rapid motion (over 40 millimeters per year) of the Hawaiian hotspot plume during Late Cretaceous to early-Tertiary times (81 to 47 million years ago). Evidence for motion of the Hawaiian plume affects models of mantle convection and plate tectonics, changing our understanding of terrestrial dynamics.

The concept of an age-progressive set of volcanic islands, atolls, and seamounts produced by a hotspot plume fixed in the deep mantle was first developed to explain the Hawaiian Islands (1). The bend separating the westward-trending Hawaiian island chain from the northward-trending Emperor Seamounts has most often been interpreted as an example of a change in plate motion recorded in a fixed-hotspot frame of reference (2).

However, global plate circuits suggest large relative motions between Hawaii and hotspots in the Atlantic and Indian Oceans (3–6). Improved mapping of marine magnetic anomalies in the Pacific has failed to define the directional change at 43 million years ago (Ma) (7) that would be expected if such a large change in plate motion had occurred. There was also a general lack of circum-Pacific tectonic events (8) documented for this time. Recent age data suggest a slightly older age for the bend [~47 Ma (9)], but this revised timing still does not correspond to an episode of profound plate motion change recorded within the Pacific basin or on its margins.

One approach to examine hotspot fixity is to determine the age and paleolatitude of volcanoes that form a given hotspot track. For the Hawaiian hotspot, the paleolatitudes of extinct volcanic edifices of the Emperor chain should match the present-day latitude of Hawaii (~19°N) if the hotspot has remained fixed with respect to Earth's spin axis. The most reliable indicators of paleolatitude are basaltic rocks, but their reliability depends on each section spanning enough time to sample geomagnetic secular variation. Recovery of such samples requires ocean-drilling technology, and only a few seamounts have been sampled to date.

Paleomagnetic analyses of 81-million-year-old basalt recovered from Detroit Seamount (Site 884) yielded a paleolatitude of ~36°N (10), which is discordant with Hawaii. Data from ~61-million-year-old basalt (9) from Suiko Seamount define a paleolatitude of 27°N (11). These data suggest that the Emperor Seamounts record southward motion of the hotspot plume in the mantle (10).

A paleomagnetic test. The Ocean Drilling Program (ODP) Leg 197 (12) sought to test the hypothesis of southward motion of the Hawaiian hotspot by drilling additional basement sites in the Emperor chain (Fig. 1). We collected detailed stepwise alternating field (AF) demagnetization data aboard the drilling ship *JOIDES Resolution*. Although these shipboard data are of high resolution, they alone are insufficient to define paleolatitudes. Magnetic minerals with intermediate to high coercivities, carrying magnetizations resistant to AF demagnetization, are commonly formed during subaerial or seafloor weathering. The magnetizations of these mineral phases are easily resolvable in thermal demagnetization data, which we also discuss here (13).

The geomagnetic field at a radius r, colatitude θ, and longitude ϕ can be described by the gradient of the scalar potential (Φ):

[1]Department of Earth and Environmental Sciences, University of Rochester, Rochester, NY 14627, USA. [2]College of Oceanic and Atmosphere Science, Oregon State University, Corvallis, OR 97331–5503, USA. [3]Geophysics Department, Stanford University, Stanford, CA 94305, USA. [4]Institute for Frontier Research on Earth Evolution, Japan Marine Science and Technology Center, Yokosuka 237–0061, Japan. [5]Department of Geology and Geophysics–School of Ocean and Earth Science and Technology, University of Hawaii, Honolulu, HI 96822, USA. [6]Department of Civil Engineering and Geological Sciences, University of Notre Dame, Notre Dame, IN 46556, USA. [7]Department of Earth, Atmospheric and Planetary Sciences, Massachusetts Institute of Technology, Cambridge, MA 02139, USA. [8]Department of Biosphere-Geosphere System Science, Okayama University of Science, Okayama 700–0005, Japan. [9]Department of Physics, Geophysics Division, University of Toronto, Mississauga, ON L5L1C6 Canada.

*To whom correspondence should be addressed. E-mail: john@earth.rochester.edu
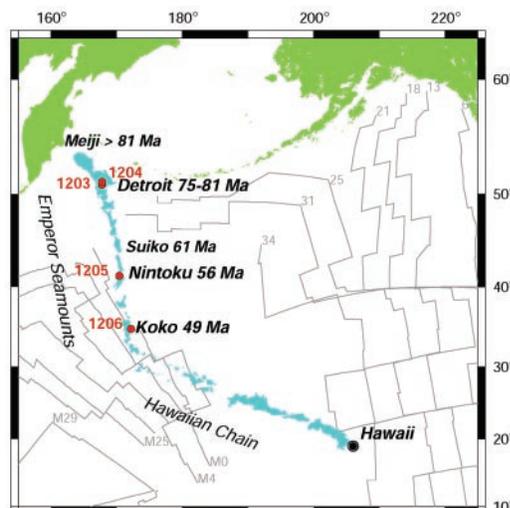
Fig. 1. Hawaiian-Emperor chain shown with ODP Leg 197 sites (12) and marine magnetic-anomaly identifications (40).

$$\Phi(r,\theta,\phi) = r_e \sum_{l=1}^{\infty} \sum_{m=0}^{l} \left(\frac{r_e}{r}\right)^{l+1} \times$$

$$P_l^m(\cos\theta)\left[g_l^m \cos m\phi + h_l^m \sin m\phi\right]$$

where P_l^m are partially normalized Schmidt functions, r_e is the radius of Earth, and the Gauss coefficients g_l^m and h_l^m describe the size of spatially varying fields. At least several millennia must be sampled such that the axial dipole term (g_0^1) becomes dominant, allowing an estimate of the paleolatitude.

We used the angular dispersion of inclination averages (*14*) from independent lava flows (inclination groups) and compared this with global lava data of the same age (*15*) to examine whether secular variation has been adequately sampled (*13*, *16*). Observations of the physical aspects of the lava flows, as well as petrologic and geochemical data, were used to group cooling units into lava units (*12*, *13*).

Marine sediments can also provide useful paleolatitude information, but they generally provide only minimum values of paleolatitude because of potential compaction-induced inclination flattening (*17*). Sediment magnetizations, however, can record long time intervals. Similarly, chemical remanent magnetizations (CRMs), carried by minerals formed during weathering, can preserve stable magnetizations that provide insight into the time-averaged field.

Koko Seamount (Site 1206). Site 1206 (Fig. 1) was positioned on the southeastern side of the lower summit terrace on Koko Seamount with the use of crossing underway seismic profiles (fig. S1). The base of the thin sediment cover contains nannofossils of Zones NP14 and NP15, which provide an early- to middle-Eocene minimum age for the volcanic basement [43.5 to 49.7 Ma (*18*)]. Fifteen volcanic formations (including pahoehoe flows, flow foot breccias, and subaerial a,a units) were recovered in 278 m of basement penetration (*12*). Thin intercalations of limestone, volcaniclastic sandstone, and a deeply weathered flow top were also recovered, providing geological evidence of time between lava flow units. The lavas are mainly of tholeiitic composition, although two alkalic flows were noted. Plateaus in ^{40}Ar/^{39}Ar incremental heating spectra from six whole-rock samples yield a mean age of 49.15 ± 0.21 Ma (2σ uncertainty quoted; table S1).

Reflected-light microscopy revealed relatively fresh titanomagnetite grains in the lavas (fig. S2A). AF demagnetization of basalt samples ($n = 74$) showed the removal of a small low-coercivity component, followed by the definition of a characteristic remanent magnetization (*12*). Two normal-polarity intervals were defined, separated by a thin reversed-polarity zone; the radiometric age data are most compatible with the chron 21n-21r-22n sequence. This assignment is confirmed by thermal demagnetization ($n = 113$), which revealed univectorial decay after the removal of a small overprint (fig. S2, B and C).

Seventeen inclination groups were identified in the thermal demagnetization data (table S2), with a mean thermal inclination ($I_T = 38.3°$ $^{+6.9°}_{-9.3°}$; hereafter, all uncertainty regions are the 95% confidence interval unless otherwise noted) that was nearly identical to that isolated by AF treatment ($I_{AF} = 38.5°$ $^{+8.4°}_{-10.9°}$, based on the 14 inclination groups sampled; (fig. S2D). The angular dispersion (*13*) of the thermal data ($S_F = 15.3°$ $^{+4.3°}_{-2.7°}$) is within the error of that predicted by global lava flows of 45 to 80 Ma (*15*). A comparison of the inclination units based on thermal demagnetization with a synthetic Fisher distribution (*19*) (Fig. 2) suggests that the basalt sequence well represents the time-averaged geomagnetic field. Furthermore, a stable magnetization carried by hematite [likely a CRM with unblocking temperatures $(T_{UB}) > 580°C$] in samples of the deeply weathered basalt yields a mean inclination ($I_T = 38.2°$ $^{+5.1°}_{-5.6°}$, $n = 10$) that is indistinguishable from that of the lava flows.

Nintoku Seamount (Site 1205). Site 1205 on Nintoku Seamount (Fig. 1) was selected with the use of two crossing seismic profiles that defined a ~43-m-thick sedimentary sequence above a flat igneous basement on the northwestern edge of the summit region (fig. S1). Nannofossils of Zone NP10 in the sediment immediately overlying the basement provide a minimum age [53.6 to 54.7 Ma (*18*)] similar to that obtained by radiometric dating of basalt from the nearby Deep Sea Drilling Project (DSDP) Site 432 [56.2 ± 0.6 Ma; 1σ error (*20*)].

A sequence of 25 subaerially erupted a'a and pahoehoe lavas and interbedded sediment and soil horizons were recovered in 283 m of basement penetration (*12*). Two flows of tholeiitic basalt are intercalated within the lower part of the sequence, which is otherwise composed of alkalic basalt. Plateaus in ^{40}Ar/^{39}Ar incremental heating spectra from six whole-rock basalt samples (table S1) spanning the section give a mean age of 55.59 ± 0.25 Ma.

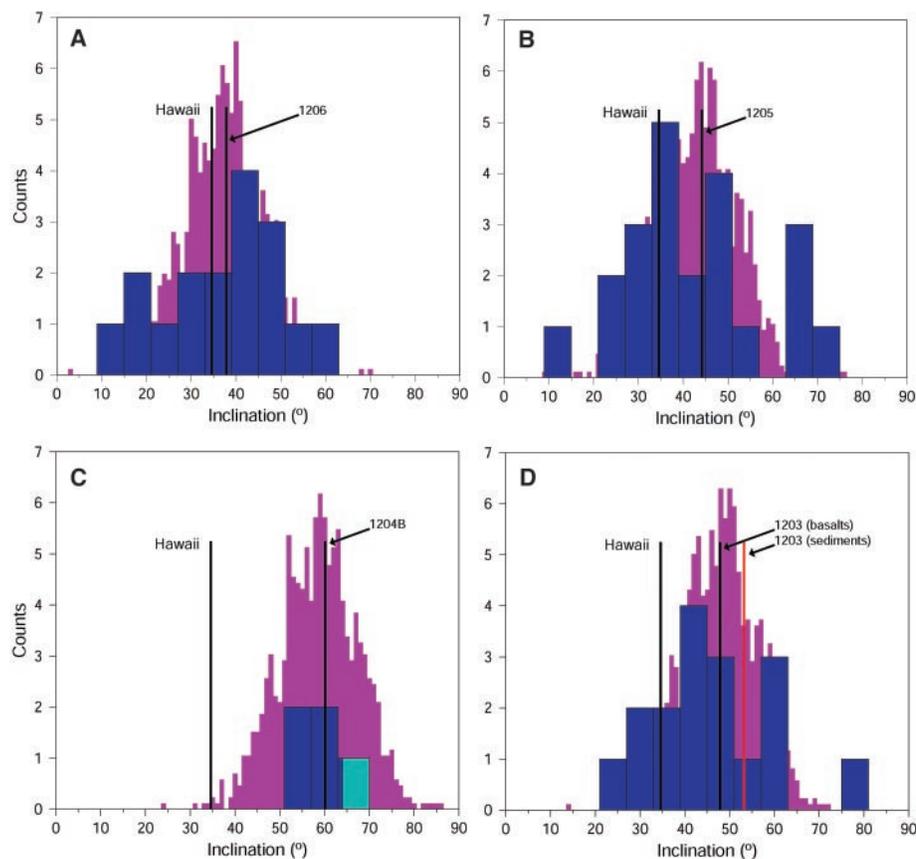**Fig. 2.** Paleomagnetic inclination groups for Sites 1206 (**A**), 1205 (**B**), 1204 (**C**), and 1203 (**D**), based on thermal demagnetization data (blue) shown compared with a synthetic Fisher distribution (magenta) that has the same mean as the experimental data and a dispersion predicted by global lava data (*15*). Latitude of Hawaii, mean basalt inclination value (thermal demagnetization) for Hole A, Site 1204 [(**C**), green], and mean sediment inclination value (thermal demagnetization) for Site 1203 (**D**) are also shown.

The recovered basalt contains fresh to slightly altered titanomagnetite grains (fig. S2E). AF demagnetization ($n = 144$) defined a reversed polarity magnetization after the removal of a normal polarity overprint. Biostratigraphic and radiometric age constraints indicate that the basalt was erupted during chron 24r (18). Thermal demagnetization of basalt samples ($n = 85$) in general showed univectorial decay after the removal of a small overprint (fig. S2F). Unblocking temperatures sometimes extended to 625°C, indicating the presence of some hematite. Low unblocking temperatures (<325°C) were seen in other samples, indicating the dominance of high-Ti titanomagnetite carriers (fig. S2G) (13).

The thermal demagnetization data (22 inclination groups) yield a mean ($I_T = -44.3°~{}^{+10.3°}_{-6.3°}$) (table S3) that is similar to that of the AF data ($I_{AF} = -45.7°~{}^{+10.5°}_{-6.3°}$) (fig. S2H). The estimated angular dispersion of the thermal data ($S_F = 19.9°~{}^{+4.8°}_{-3.2°}$) is higher than that predicted by models (15) based on the average data of lavas from 45 to 80 Ma, and may point to higher frequency changes in secular variation with time. Nevertheless, the geologic evidence for time, together with a comparison of the data versus a Fisherian distribution (Fig. 2), suggests that the mean value represents the time-averaged field.

Detroit Seamount (Site 1204). Site 1204 (Fig. 1) was chosen along two crossing seismic profiles that revealed a flat basement surface beneath ~850 m of sediments (fig. S1). Two holes were drilled (A and B), penetrating 60 and 138.5 m of basalt, respectively. Diamictite and volcanic ash–rich sediment directly overlying the basement contain Campanian nannofossils (CC22/23) of ~73 to 76 Ma (19); nannofossils of this zone were also recovered in a sediment interbed in the last core from Hole B, suggesting that the entire basement section drilled is of this age (12).

The basement units are pillow lavas consisting of multiple lobes (which are sometimes separated by calcareous sediment) intercalated with a 46-m-thick interval of massive lava (diabase) and a 10-m-thick hyaloclastite lapilli breccia interval (12). The basalt has undergone low-temperature alteration, consistent with late-stage seafloor weathering. $^{40}Ar/^{39}Ar$ incremental heating spectra from four whole-rock basalt samples and a feldspar separate failed to show plateaus in the step-heating ages. The apparent ages for total fusion range from 33 to 58 Ma, indicating variable loss of radiogenic ^{40}Ar (table S1).

Reflected-light microscopy showed a dominance of titanomaghemite in basalt samples (fig. S2I). Linear decay during AF demagnetization was observed in only ~70% of the samples examined (Hole A: $n = 9$; Hole B: $n = 39$). In these cases, a normal polarity

magnetization was defined (12). Thermal demagnetization, however, revealed a clear two-component structure in many samples (13). A reversed-polarity component was defined at low unblocking temperatures (T_{UB} ranging from 100°C to between 275° and 350°C), whereas a normal-polarity component was defined at higher temperatures (fig. S2, J and K). We interpret the high T_{UB} component as the primary magnetization because it is the only magnetization seen in the least altered rocks after the removal of viscous components; we believe the reversed-polarity component is a later magnetization carried by titanomaghemite.

We identified only a single inclination unit in Hole A. Thermal demagnetization data ($n = 10$) yield a mean inclination ($I_T = 64.5°{}^{+10.2°}_{-19.0°}$) that differs from that observed by AF treatment ($I_{AF} = 55.5°~{}^{+6.8°}_{-8.3°}$), presumably because the latter fails to separate the two components of magnetization. On the basis of a lithofacies succession in Hole B (12), we identified five inclination groups. Our thermal results ($n = 36$) indicate a mean inclination of $60.1{}^{+5.2°}_{-5.5°}$ ($I_{AF} = 58.9°{}^{+5.8°}_{-6.4°}$, based on AF data) for Hole B (table S4 and fig. S2L). Angular-dispersion estimates are low ($S_F = 3.1°~{}^{+2.0°}_{-0.9°}$) and at face value suggest that the sequence does not adequately sample secular variation (Fig. 2). However, rather than random directions, AF and thermal demagnetization of breccia samples often revealed a consistent normal-polarity direction, similar to that of the basalt flows. This observation, together with the presence of titanomaghemite, suggests that CRMs might be important at this site.

Detroit Seamount (Site 1203). Site 1203 (Fig. 1) on Detroit Seamount was located in an area of flat basement imaged in three crossing seismic lines (fig. S1). A thick (462-m) pelagic sedimentary sequence overlies the basement. Eighteen compound lava-flow units and 14 volcaniclastic sedimentary interbeds were drilled in 453 m of basement penetration (12). Nannofossils of Zone CC22 were identified in sedimentary beds within the basement sequence, indicating an age of 75 to 76 Ma (12). Plateaus in $^{40}Ar/^{39}Ar$ incremental heating spectra from three whole-rock basalt samples and two feldspar separates (table S1) yield a mean age of 75.82 ± 0.62 Ma.

The upper part of the basement sequence consists of nonvesicular pillow lavas and thick, sparsely vesicular pahoehoe lava flows. These lavas were deposited far from eruptive centers at relatively shallow depths (fig. S1). The lower part of the sequence is dominated by highly vesicular compound pahoehoe lavas (up to 65 m thick) but also contains pillow lavas and hyaloclastite, indicative of shallow marine to subaerial environments. Tholeiitic to transitional basalt dominates

the section, but some alkali basalt is intercalated in the lower sequence. This occurrence of alkalic lavas is unexpected; it may indicate the interfingering of volcanoes in different stages of evolution, as can be seen today between Mauna Loa and Mauna Kea on Hawaii.

The lavas have a range of magnetic mineralogies, from relatively fresh titanomagnetite to grains showing titanomaghemitization (fig. S2M). AF demagnetization of most of the basalt samples ($n = 199$) and sediment samples ($n = 34$) that we examined showed a stable single component of normal polarity after the removal of a low-coercivity (<10-mT) overprint (12). In the two uppermost flows, AF demagnetization patterns were more complex, indicating the presence of additional, unresolved components. Titanomaghemite, detected by reflected light microscopy, is common in the upper flows.

Thermal demagnetization data of lava samples ($n = 87$) (fig. S2N) and sediment samples ($n = 28$) (fig. S2O) mostly showed univectorial decay after the removal of a small overprint at low unblocking temperatures. In the two uppermost flows of the sequence, however, a distinct reversed component of magnetization was isolated (T_{UB} ranging from ~100° to between 250° and 325°C) before definition of a normal polarity magnetization at higher temperatures. As in the Site 1204 basalts, we interpret the higher T_{UB} magnetization as the primary remanence.

Thermal demagnetization results from lava samples (16 inclination groups) yield a mean ($I_T = 48.6°~{}^{+7.0°}_{-10.6°}$; table S5) similar to that calculated from the AF data ($I_{AF} = 50.0°~{}^{+7.3°}_{-10.6°}$, for 14 inclination units, excluding the uppermost lava flows; fig. S2P). The estimated angular dispersion of the thermal demagnetization data ($S_F = 18.4°~{}^{+6.9°}_{-3.7°}$) is slightly higher than that expected from global lava-flow data (15) (Fig. 2). The inclination average from AF demagnetization of sediment samples ($I_{AF} = 54.7°~{}^{+3.1°}_{-6.4°}$) (12, 13) is confirmed by thermal demagnetization ($I_T = 53.2°{}^{+5.0°}_{-11.4°}$) and is somewhat steeper than the basalt mean.

Paleolatitude history. The inclination groups, averaged by site, form a progressive sequence of decreasing paleolatitudes with time (Fig. 3) that is inconsistent with the fixed-hotspot hypothesis. We did not recover coral reef material north of Koko Guyot (nor did we find evidence of such material as sedimentary debris). This is consistent with the idea that the hotspot was once located farther north, beyond the latitudinal zone supporting reef growth (21).

Four data sets are now available from Detroit Seamount based on thermal demagnetization (Fig. 3). Lava emplacement may

have been less frequent at Site 884 relative to the other sites because of its flank position. The Site 1204 (Hole B) lavas record a low angular dispersion, but these rocks might carry a CRM, explaining the agreement of their mean inclination with that of the Site 884 basalt section and the Site 1203 sediments. Because of potential inclination shallowing, the mean inclination from the Site 1203 sediments should be a minimum. This suggests further that the mean derived from the basalts at the same site is shallower because the available lavas underrepresent higher inclination values.

We consider two scenarios: one in which the paleomagnetic results from the Site 884 basalts, 1204 (Hole B) basalts, and Site 1203 sediments best represent the field (paleolatitude model A; $I_T = 56.5° \, ^{+12.4°}_{-12.6°}$, $N = 3$) and another in which we combine all the individual basalt inclination units from Detroit Seamount into a mean (Model B; $I_T = 52.9°$ $^{+3.7°}_{-6.9°}$, $N = 32$). With either model, the paleolatitude and age data yield average rates (Model A: 57.7 ± 19.2 mm year^{-1}; Model B: 43.1 ± 22.6 mm year^{-1}) that are consistent with the hypothesis that the Hawaiian hotspot moved rapidly southward from 81 to 47 Ma (10). The values are consistent with updated estimates of hotspot motion based on independent relative plate motions (5). Both paleolatitude models suggest that most of the motion occurred before the time of the Hawaiian-Emperor bend (Model A, >44 Ma; Model B, >43 Ma). This is further supported by the mean paleolatitude value from Koko Seamount (based on both thermoremanent magnetizations and CRMs), which is only 2.5° north of the fixed-hotspot prediction.

Modeling of hotspot motion. Crust ages available from marine magnetic anomalies, radiometric age data from drill sites, and geochemical data (22) indicate that the Hawaiian hotspot was close to a spreading ridge during the formation of Detroit Seamount (23). Hence, asthenospheric channeling of the plume (24) from a position to the south toward a more northerly ridge could have played some role in the difference between the paleomagnetic data and the prediction of the fixed-hotspot model. The monotonic age progression of lavas recovered from Detroit to Koko Seamounts, however, leads us to believe that this potential channeling of plume material was limited to the region at or north of Detroit Seamount. Furthermore, the similarity of the Hawaiian-Emperor chain with the Louisville chain of the South Pacific suggests that asthenospheric channeling was not the sole cause of the paleolatitude progression.

We examined whether the observed paleolatitude motion can be explained by a geodynamic model of the interaction of a plume with large-scale mantle flow. The flow

calculation (25) requires a mantle density and viscosity model and a surface-velocity boundary condition (13). A tomography model was used to infer mantle density variations (26), and a viscosity structure based on an optimized fit to the geoid (with additional constraints from heat flow) (27) was applied. Both moving- and fixed-plume sources (28, 29) that originate at the top of the low-viscosity layer at the base of the mantle were considered (13).

Fast motion occurs when a conduit is sheared and tilted in the large-scale flow and the tilted conduit rises to the surface aided by

a large-scale upwelling. Thus, in these models, fast hotspot motion corresponds to slower mantle flow rates (~10 to 20 mm year^{-1}). Most computations (25) yield a hotspot motion of 5° to 10° toward the south to southeast during the past 100 million years (My). It is possible to achieve a good fit to the paleomagnetic data, because the age of the initiation of the Hawaii hotspot is unknown (and can hence be used as a free parameter). For the moving-source model, southward motion tends to be faster if an earlier plume origin is assumed. However, plume initiation ages from 180 to 120 Ma (which imply the sub-
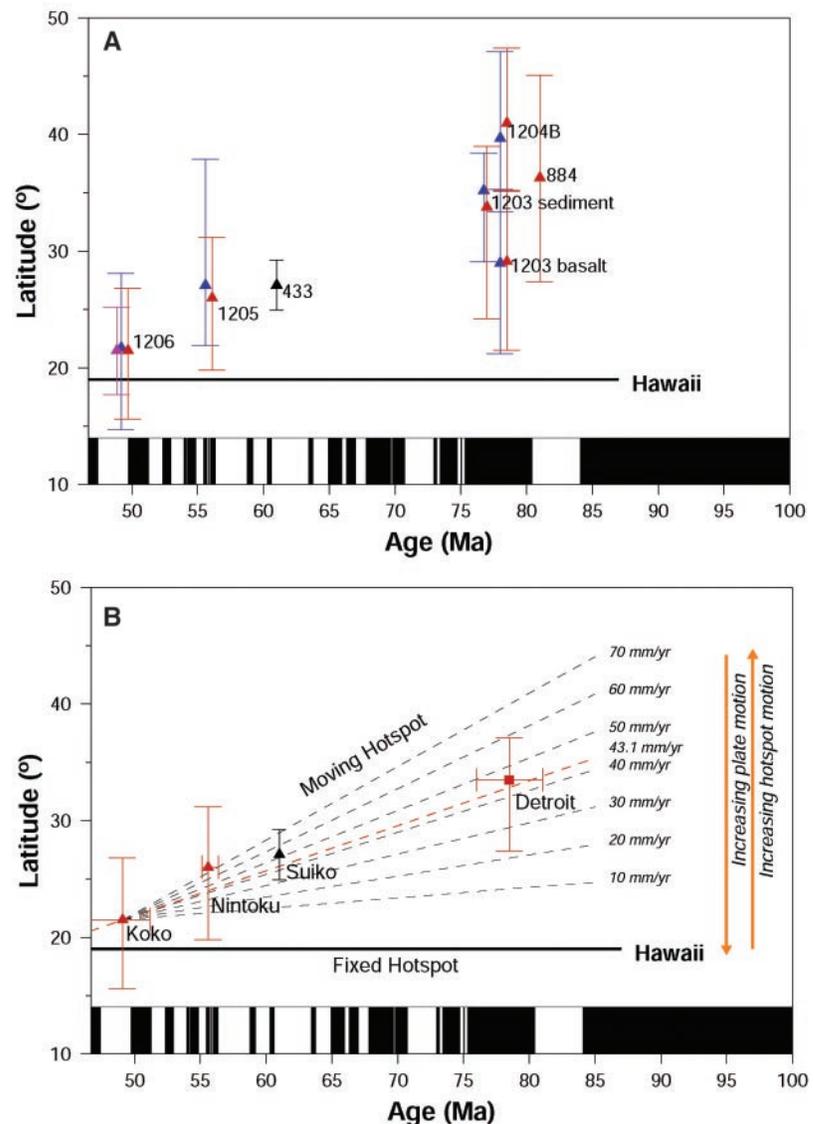

Fig. 3. (**A**) Paleolatitude data from ODP Leg 197 sites (1206, Koko Seamount; 1205, Nintoku Seamount; 1204B and 1203, Detroit Seamount), ODP Site 884 (Detroit Seamount) (10), and DSDP Site 433 (Suiko Seamount) (11). Orange, results of thermal demagnetization; blue, results of alternating field demagnetization. Result from 433 is based on AF and thermal data. Magenta, magnetization carried by hematite from weathered basalt from Site 1206. (**B**) Average paleolatitude value for Detroit Seamount (square), based on inclination groups derived from basalts of Sites 884, 1203, and 1204B (Model B, see text), plotted with select values from other seamounts (A). Also shown is a least-squares fit to the data (orange) and several paleolatitude trajectories representing combinations of plate and hotspot motion.

1067

duction of volcanic edifices older than the oldest extant seamount, Meiji Guyot) generally yield the best fits. For the fixed-source model, the computed hotspot motion consists of two distinct phases. During the first phase, which lasts 100 to 150 My, southward motion can be rapid. The second phase begins when the first conduit elements that arise from the fixed source reach the surface. The computed hotspot motion is slow during the second phase and, in the example shown (Fig. 4), somewhat toward the north (13).

Overall, the results of the large-scale flow modeling approach described above are consistent with the Leg 197 paleomagnetic data. Potentially important differences lie in the total motion predicted since ~80 Ma (13) and in the need to incorporate in the modeling results a change in plate motion at or near the time of the bend. The paleomagnetic data do not require a change in plate motion, although a small change is not excluded.

Implications of hotspot motion. The hotspot motion defined by the new paleomagnetic and radiometric age data has implications for a wide variety of issues, including true polar wander (TPW) (30), the morphology of the past geomagnetic field, and the history of plate motions. Some investigators (31) have proposed that as much as 30° of TPW (rotation of the entire solid Earth) has accumulated during the past 200 My. However, a fixed-hotspot reference frame is used to define TPW in these studies. The data presented here, together with other tests (32, 33), indicate that TPW has been overestimated; Earth has been relatively stable with re-

spect to the spin axis since the Early Cretaceous Epoch. Similarly, some changes in the morphology of the geomagnetic field with time (34) that have relied on fixed hotspots to anchor data from global sites are probably artificial. One recent analysis that has not relied on the fixed-hotspot reference frame has called for a significant axial octopole contribution (g_0^3) to the time-averaged field (35). This conclusion is controversial, but if correct, it would imply that our paleolatitude calculations underestimate the true hotspot motion.

Backtracking the position of early-Tertiary and older Pacific basin sites, an essential aspect of some paleoclimate and tectonic studies, requires rethought, given that previous efforts have also relied on fixed hotspots. The northerly position of the Late Cretaceous Hawaiian hotspot (23) casts doubt on the southern option for the Kula-Farallon ridge [a plate configuration that is typically called on to create high rates of northward transport for tectonostratigraphic terranes in Alaska and British Columbia (36, 37)].

The fixed-hotspot interpretation of the Hawaiian-Emperor bend implies that huge plates can undergo large changes in direction rapidly. But such changes cannot be associated with internal buoyancy forces (such as subducting slabs) because these require many millions of years to develop. This has led to the suggestion that plate-boundary forces might be responsible (38). The new paleolatitude and radiometric age data (9) suggest that changes of plate motion at the time of the Hawaiian-Emperor bend were much smaller

and more gradual than previously thought. Given the central role the Hawaiian-Emperor bend has played as an example of plate motion change, these observations now raise the question of whether major plates can undergo large changes in direction rapidly, and whether plate boundary forces alone can play a dominant role in controlling plate motion.

The similarity of the Hawaiian and Louisville hotspot tracks implies that the motion we are tracking by the new paleomagnetic data is of large scale. This Late Cretaceous to early-Tertiary episode of hotspot motion was not isolated; motion of the Atlantic hotspots relative to those in the Pacific occurred at similar rates during mid-Cretaceous times (39). These data sets indicate a much more active role of mantle convection in controlling the distribution of volcanic islands. At times, it is this large-scale mantle convection that is the principal signal recorded by hotspot tracks.

References and Notes

1. J. T. Wilson, *Can. J. Phys.* **41**, 863 (1963).
2. W. J. Morgan, *Nature* **230**, 42 (1971).
3. P. Molnar, T. Atwater, *Nature* **246**, 288 (1973).
4. P. Molnar, J. Stock, *Nature* **327**, 587 (1987).
5. C. A. Raymond, J. M. Stock, S. C. Cande, in *The History and Dynamics of Global Plate Motions*, vol. 121, *Geophysical Monograph Series*, M. A. Richards, R. G. Gordon, R. D. van der Hilst, Eds. (American Geophysical Union, Washington, DC, 2000), pp. 359–375.
6. V. DiVenere, D. V. Kent, *Earth Planet. Sci. Lett.* **170**, 105 (1999).
7. T. Atwater, in *The Eastern Pacific Ocean and Hawaii*, vol. N of *The Geology of North America*, E. L. Winterer, D. M. Hussong, R. W. Decker, Eds. (Geological Society of America, Boulder, CO, 1989), pp. 21–72.
8. I. O. Norton, *Tectonics* **14**, 1080 (1995).
9. W. D. Sharp, D. A. Clague, *Eos* **83**, F1282 (2002).
10. J. A. Tarduno, R. D. Cottrell, *Earth Planet. Sci. Lett.* **153**, 171 (1997).
11. M. Kono, *Init. Rep. Deep Sea Drill. Proj.* **55**, 737 (1980).
12. J. A. Tarduno et al., *Proceedings of the Ocean Drilling Program, Initial Report* (Ocean Drilling Program, College Station, TX, 2002), vol. 197.
13. Material and methods are available as supporting material on *Science* Online.
14. P. L. McFadden, A. B. Reid, *Geophys. J. R. Astron. Soc.* **69**, 307 (1982).
15. P. L. McFadden, R. T. Merrill, M. W. McElhinny, S. Lee, *J. Geophys. Res.* **96**, 3923 (1991).
16. A. V. Cox, *Geophys. J. R. Astron. Soc.* **20**, 253 (1970).
17. J. A. Tarduno, *Geophys. Res. Lett.* **17**, 101 (1990).
18. W. A. Berggren, D. V. Kent, C. C. Swisher III, M.-P. Aubry, *Soc. Econ. Paleontol. Mineral. Spec. Publ. 54* (1995), pp. 129–212.
19. R. A. Fisher, *Proc. R. Soc. London Ser. A* **217**, 295 (1953).
20. G. B. Dalrymple, M. A. Lanphere, D. A. Clague, *Init. Rep. Deep Sea Drill. Proj.* **55**, 659 (1980).
21. J. McKenzie, D. Bernoulli, S. O. Schlanger, *Init. Rep. Deep Sea Drill. Proj.* **55**, 415 (1980).
22. R. A. Keller, M. R. Fisk, W. M. White, *Nature* **405**, 673 (2000).
23. R. D. Cottrell, J. A. Tarduno, *Tectonophysics* **362**, 321 (2003).
24. C. J. Ebinger, N. H. Sleep, *Nature* **395**, 788 (1998).
25. B. Steinberger, *Geochem. Geophys. Geosyst.* **3**, 10.1029/2002GC000334 (2002).
26. T. W. Becker, L. Boschi, *Geochem. Geophys. Geosyst.* **3**, 10.129/2001GC000168 (2002).
27. B. M. Steinberger, A. R. Calderwood, paper presented at the European Union of Geosciences XI meeting, Strasbourg, France, 8 to 12 April 2001.
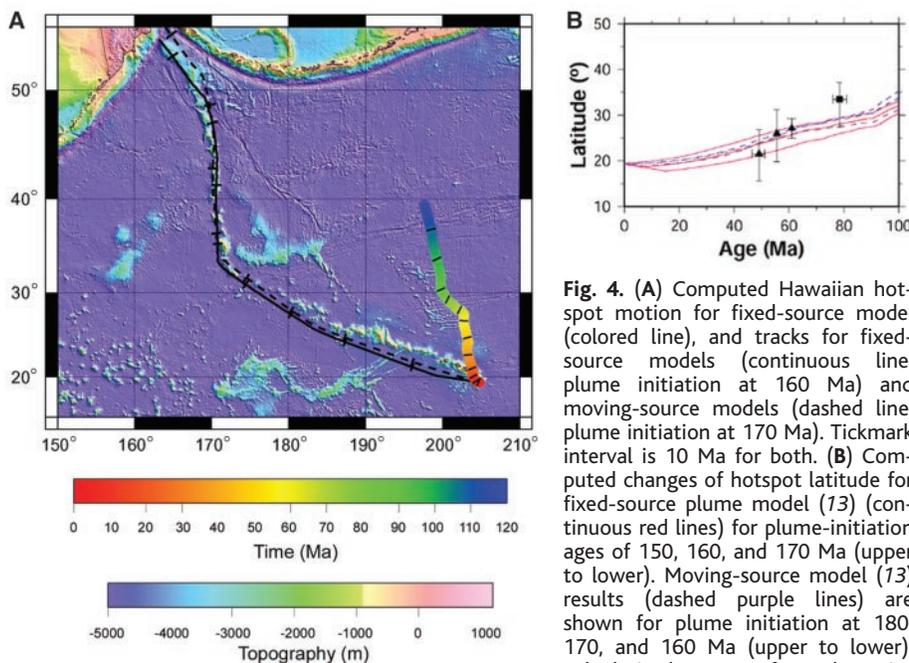28. A. M. Jellinek, M. Manga, *Nature* **418**, 760 (2002).

Fig. 4. (A) Computed Hawaiian hotspot motion for fixed-source model (colored line), and tracks for fixed-source models (continuous line; plume initiation at 160 Ma) and moving-source models (dashed line; plume initiation at 170 Ma). Tickmark interval is 10 Ma for both. **(B)** Computed changes of hotspot latitude for fixed-source plume model (13) (continuous red lines) for plume-initiation ages of 150, 160, and 170 Ma (upper to lower). Moving-source model (13) results (dashed purple lines) are shown for plume initiation at 180, 170, and 160 Ma (upper to lower). Paleolatitude means for Koko, Nintoku, Suiko, and Detroit Seamounts (Fig. 3) are also shown.

29. A. Davaille, F. Girard, M. Le Bars, *Earth Planet. Sci. Lett.* **203**, 621 (2002).
30. P. Goldreich, A. Toomre, *J. Geophys. Res.* **74**, 2555 (1969).
31. J. Besse, V. Courtillot, *J. Geophys. Res.* **107**, 10.1029/2000JB000050 (2002).
32. J. A. Tarduno, A. V. Smirnov, *Earth Planet. Sci. Lett.* **184**, 549 (2001).
33. J. A. Tarduno, A. V. Smirnov, *Earth Planet. Sci. Lett.* **198**, 5533 (2002).
34. R. A. Livermore, F. J. Vine, A. G. Smith, *Geophys. J. R. Astron. Soc.* **79**, 939 (1984).
35. R. Van der Voo, T. H. Torsvik, *Earth Planet. Sci. Lett.* **187**, 71 (2001).
36. D. C. Engebretson, A. V. Cox, R. G. Gordon, *Geol. Soc. Am. Spec. Pap. 206* (1985), pp. 1–59.
37. H.-P. Bunge, S. P. Grand, *Nature* **405**, 337 (2000).
38. M. A. Richards, C. Lithgow-Bertelloni, *Earth Planet. Sci. Lett.* **137**, 19 (1996).
39. J. A. Tarduno, J. Gee, *Nature* **378**, 477 (1995).
40. R. D. Mueller, W. R. Roest, J.-Y. Royer, L. M. Gahagan, J. G. Sclater, *J. Geophys. Res.* **102**, 3211 (1997).
41. This research used samples provided by the ODP, which is sponsored by NSF and participating countries under management of the Joint Oceanographic Institutions. We thank the scientific and operational parties of Leg 197 for their contributions at sea; the staff of ODP–Texas A&M University for their techni-cal support; and P. Doubrovine, G. Olton, D. Sinnett, and A. O'Kane for assistance with magnetic measurements. Supported by NSF.

Hairpin RNAs and Retrotransposon LTRs Effect RNAi and Chromatin-Based Gene Silencing

Vera Schramke and Robin Allshire*

The expression of short hairpin RNAs in several organisms silences gene expression by targeted mRNA degradation. This RNA interference (RNAi) pathway can also affect the genome, as DNA methylation arises at loci homologous to the target RNA in plants. We demonstrate in fission yeast that expression of a synthetic hairpin RNA is sufficient to silence the homologous locus in trans and causes the assembly of a patch of silent Swi6 chromatin with cohesin. This requires components of the RNAi machinery and Clr4 histone methyltransferase for small interfering RNA generation. A similar process represses several meiotic genes through nearby retrotransposon long terminal repeats (LTRs). These analyses directly implicate interspersed LTRs in regulating gene expression during cellular differentiation.

Eukaryotic genomes invariably contain repetitive DNA sequences of uncertain functional significance: large expanses of heterochromatin are associated with centromere regions and flank the kinetochores at centromeres. This centromeric heterochromatin is frequently made up of tandem arrays of simple satellites interspersed with transposable elements (*1–5*). Moreover, recent studies support a direct role for such tandem repeats in centromere function, because arrays of human centromeric α-satellite allow de novo kinetochore assembly (*1*). In addition, the heterochromatin that coats centromeric repeats in fission yeast (*Schizosaccharomyces pombe*) plays an important role in sister-centromere cohesion (*6, 7*).

Other repetitive elements (e.g., retrotransposons) are found scattered throughout eukaryotic genomes (*8*). It is becoming apparent that interspersed repeats can influence the expression of nearby genes (*9, 10*). McClintock first recognized this potential role for transposons in maize and referred to them as controlling elements (*11*). Consistent with this, mutations that reduce DNA methylation in plants result in activation and mobilization of transposons and lead to epimuta-tions (*12, 13*). Although transposable elements can alter the expression of neighboring genes in plant and animal cells (*8–10*), it remains unclear whether these elements play a direct role in endogenous gene regulation. Nevertheless, early models proposed that families of interspersed repetitive sequences might regulate networks of genes and lead to cellular differentiation in response to a signal (*14*).

The heterochromatic nature of centromeres and the abundance of transposable elements at pericentromeric regions in some organisms suggests links between transposon silencing and centromeric heterochromatin formation. In mammalian cells, both centromeric and retrotransposon repeats have a similar repertoire of both DNA and chromatin modifications that are usually found associated with silent chromatin and also attract cohesin (*15–18*).

Fission yeast centromeres are composed of outer repeats that flank the central kinetochore domain. Marker genes placed within these repeats are silenced by a process requiring Clr4, which methylates histone H3 on lysine 9 (MeK9-H3), which allows binding of Swi6 (the ortholog of metazoan HP1) and Chp1 to these outer repeats (*19–24*). Overlapping noncoding transcripts are produced from these repeats, and analyses suggest that their processing by the RNA interference (RNAi) machinery results in the generation of small interfering RNAs (siRNAs), which are continually required for the formation of silent chromatin over these centromere repeats (*25, 26*) and for centromere function (*27–29*). Proteins related to CENP-B and the mariner class of transposases also bind the outer repeat sequences at fission yeast centromeres and contribute to the formation of heterochromatin (*30*). In addition to centromeric repeats, the standard fission yeast genome contains 13 intact Tf2 retrotransposable elements plus 249 Tf1 and Tf2 long terminal repeats (LTRs), or related LTRs, and LTR fragments dispersed throughout the genome (*31*).

In many organisms, the process of RNAi has been exploited to nullify gene expression (*32*). Silencing can occur in two ways: posttranscriptional gene silencing (PTGS) involves degradation of the targeted RNA; studies in plants indicate that expression of double-stranded RNAs (dsRNAs) can result in DNA methylation and transcriptional gene silencing (TGS) at the target locus (*33–35*). Moreover, the RNAi pathway is required for the generation of siRNAs homologous to, and DNA methylation of, retrotransposons in plants (*36, 37*). Here we test whether, in fission yeast, the RNAi machinery is preserved to specifically process transcripts generated from centromeric repeat sequences or if it can act to silence noncentromeric transcripts in trans and trigger heterochromatin formation. We also demonstrate that endogenous, developmentally regulated, lineage-restricted genes are subject to control by this same process and that adjacent retrotransposon LTRs effect this regulation.

Short hairpin RNA (shRNA) can silence a normally expressed *ura4*⁺ gene. To determine whether the RNAi machinery of fission yeast can act to process noncentromeric repeat transcripts, we cloned an internal region [280 base pairs (bp) of *ura4*⁺, Stu I–Eco RV (SE)] from the *ura4* open reading frame (ORF) in an inverted orientation around a 355-bp spacer under the control of the *nmt*41 promoter (*shuraSE*; Fig. 1A). To assess whether expression of *shuraSE* could induce silencing of the *ura4*⁺ gene, we transformed the construct and empty vector into two strains; one in which the endogenous *ura4*⁺ locus remained intact and the other in which the 280-bp Stu I–Eco RV region was deleted from the *ura4* gene (*ura4-DS/E*, which lacks homology to *shuraSE*) and a wild-type copy of *ura4*⁺ had been inserted at another location (*Rint:ura4*⁺). Previous analyses demon-

Wellcome Trust Centre for Cell Biology, Institute of Cell and Molecular Biology, King's Buildings, University of Edinburgh, Edinburgh EH9 3JR, Scotland, UK.

*To whom correspondence should be addressed. E-mail: robin.allshire@ed.ac.uk